International Journal of Electronics Engineering, 1(1), 2009, pp. 19-26

Features Preserved Medical Image Denoising Using Steered Complex Shrinkage Algorithm

M. Venu Gopala Rao[1] & S. Vathsal[2]

[1]*Narasaraopeta Engineering College, Narasaraopet, Guntur Dt., A. P., INDIA*

[2]*Director, Dept. of Energy, VIT University, Vellore, T. N., INDIA*

Abstract: *In this paper we propose a new wavelet domain, structure driven denoising technique called* ***Steered Complex*** Shrinkage *which preserves the edges, corners and orientation features and application to medical images. For this purpose we used an efficient steerable complex pyramidal wavelet transform that uses pairs of complex steerable orientation bandpass filters. These complex filters have been engineered into a multirate system, providing a synthesis and analysis sub band filtering system with good reconstruction properties. The performance of the proposed denoising algorithm is comparable with that of recently reported state-of-the-art denoising techniques using undecimated discrete wavelet transform with soft-shrinkage, and presents a very promising avenue for exploring structure based denoising in the wavelet domain.*

Keywords*: Steerable filters, Complex steerable pyramid wavelet transform, edge, corner and oriented features, Medical image Denoising.*

1. INTRODUCTION

Estimates of local orientation in images play a very important role in many computer vision tasks such as feature detection, image denoising, contour extraction, image segmentation and even high-level tasks such as object recognition. Local orientation may be estimated from the vector fields obtained by applying differential operators, edge detectors [1], [19] and steerable filters [18] to the luminance channel of a colour image.

In medical images, noise suppression is particularly a delicate and difficult task. A trade off between noise reduction and the preservation of actual features (such as edges, corners, and orientations) has to be made in a way that enhances the diagnostatically relevant image content. Image processing specialist usually lack of biomedical expertise to judge the diagnostic relevance of the denoising results. For example, in MRI images corrupted by Rician noise may contain information useful to medical experts. And also biomedical images show extreme variability and it is necessary to operate on a case by case basis. This motivates us the co-nstruction of denoising methods that preserves the important features of medical images. In this paper we propose a wavelet domain structural driven denoising technique called *Steered Complex Shrinkage* using steerable pyramid complex wavelet transform.

1.1 Motivation and Background

In the past two decades there has been a fair amount of research on wavelet thresholding and threshold selection for signal denoising because wavelet provides an appropriate basis for separating noisy signal from the image signal. These classical discrete wavelet transforms (DWT) are non-redundant, and are powerful tools for many non-stationary signal processing applications, but they suffers from the following major limitations; (i) oscillations (ii) shift sensitivity (iii) poor directionality, (iv) rotation invariance and (v) absence of phase information. To overcome these limitations many researchers are developed various techniques. For example Freeman [1] introduced steerable filters and Simoncelli [2] further developed and introduced shift-invariant transform employing undecimated band pass filters. More recently Kingsbury [3] introduced a very elegant computational structure, the dual tree complex wavelet transform (DT-DWT) which employs near-shift (rather than rotation) invariant properties. Recently, we proposed a hybrid algorithm named as a Complex Fourier Wavelet regularized Deconvolution (ComForWaRD) algorithm [4] for medical imaging using DT-DWT and proved that it outperforms in all aspects with that of recently reported state-of-the-art denoising techniques using undecimated discrete wavelet transform with soft shrinkage. Other constructions can be found such as [5] and [6]. The main limitations in both steerable pyramid and DT-DWT of Kingsbury's approach is that they employ over-complete represent-tations and computationally intensive. And also their performance in compression process is poor.

Orientation estimation is particularly important for the extraction of contour or region boundaries for image segmentation. Although in signal processing, the dominant orientation is usually dependent on the size or scale of a given

*Corresponding author: mvgr03@gmail.com; svathsal@gmail.com

neighbourhood, human subjects perceive contour boundaries and their orientations at the appropriate scale for segmentation. This indicates that a scale selection or a scale weighting process is involved in the human perception of orientation, especially for boundaries. Perona [20] applied anisotropic diffusion to orientation maps. Feng and Milanfar [21] used principle Component Analysis (PCA) to obtain the dominant orientation at each scale and weighted these with an eigenvalue based measure of orientation dominance. This yields a single orientation estimate for each location. Solving eigen systems of gradient neighbor hoods for each location and scale adds a computational overhead and the particular measure of orientation dominance is limited by the evaluation of gradient energy in only two orthogonal orientations, i.e. the method assumes a maximum of two orthogonal structures at each location. We adopt a different approach by increasing the orientation-selectivity of our filters such that the interference from structures at different orientations is minimized, thereby avoiding the need to solve eigen systems at each scale.

We propose an effective and feature preserving denoising technique using steerable pyramid complex wavelet transform originally proposed by A.A. Bharath and Jeffry Ng [7]. This transform has two important features: (i) the filter kernels are specified by separable angular and radial functions in the frequency domain which has not been reported jointly in a multirate scheme so far, and (ii) transform domain denoising system which exploits steerability property explicitly.

1.2 Filtering Adopted to Expert Defined Features of Interest

Clinicians usually tend to prefer the original noisy images (for example ultrasound) rather than the smoothed versions because the filters, no matter how sophisticated they are, can destroy some relevant image details. However, it is also true that noise suppression in many cases significantly enhances the visibility of some image features and it undoubtedly facilitates automatic image processing tasks such as segmentation. It is thus important to develop such noise filters, which can guarantee the preservation of those features that are of interest to the clinician.

The paper is organized as follows. The structure of Steerable Complex Pyramid Wavelet Transform is briefly outlined in Section-2. The orientation maps, corner likelihood response, phase and edge structure estimations are described in Section-3. The denoising algorithm *using Steered Complex Shrinkage Technique* is described in Section-4. The computer simulations and results for CT and MR images are discussed in Section-5, Finally the conclusions and further research is provided at the end.

2. STEERABLE COMPLEX PYRAMID WAVELET TRANSFORM

The design of the pyramid employs decimation in the lowpass channel in order to achieve the scaling of filter responses through successive levels of decomposition. The nature of the scheme is illustrated in Fig.1. For convenience in tuning angular and radial characteristics of the filters, we impose Fourier domain polar separability, so that an analysis filter $G_{0,k}(\omega, \phi)$ in the kth direction in a filter set can be specified as the product of a radial frequency function and $\Omega_0(\omega)$ angular frequency function $\Phi_{0,k}(\phi)$, i.e., $G_{0,k}(\omega, \phi) = \Omega_0(\omega)\Phi_{0,k}(\phi)$. The matching synthesis filter $G_{1,k}(\omega, \phi)$ can be specified by the product of the same angular frequency function $\Phi_{0,k}(\phi)$ and a synthesis radial frequency function $\Omega_1(\omega)$.

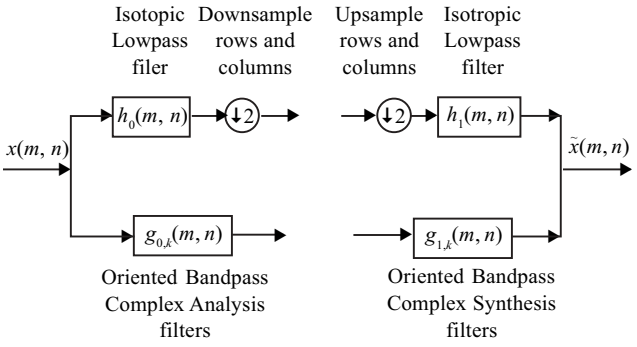

Figure 1: Isotropic Representation of Pyramidal Unit, Illustrating a Single Stage of Decomposition and Reconstruction

2.1 Radial Frequency Response of the Lowpass Filters

The isotropic low-pass radial frequency response, in the radial frequency domain on the interval $-\pi < \omega \le \pi$ is given by

$$H_0(\omega, \phi) = H_0(\omega) = \frac{1}{1 + (\omega / \omega_c)^6} \tag{1}$$

where $\omega_c = 3\pi/8$. This is equivalent to a cascade of two third-order Butterworth filters, and was chosen to provide a reasonably flat power response, when used in combination with the bandpass radial frequency response, for radial frequency components in the range $[0, \omega_{max}]$. The value ω_{max} resents the maximum frequency of the bandpass radial frequency response.

2.2 Radial Frequency Response of the Bandpass Filters

For most natural scenery, the magnitude of the frequency components drops off rapidly with increasing radial spatial frequency. With this choice of lowpass filter characteristic, the aliasing is minimal, except in the high-frequency components images. The radial frequency response of the bandpass filters is based on Erlang functions (further details see [8]) is given by

$$\Omega_0(\omega) = \left(\frac{e}{14}\right)^7 \omega^7 e^{-\omega/2} U(\omega) \tag{2}$$

where $U(\omega)$ is the unit step function. Erlang functions are one sided, are smooth, and have the property that $\Omega_0(\omega) = 0$.

2.3 Angular Frequency Response

The angular characteristics of the steerable wavelets are determined by several requirements. First, the requirement to achieve near-perfect reconstruction (PR) in the angular decomposition is desirable. The filters that we have designed use, instead, a function that is zero over one half of Fourier space. This yields complex filters consisting of symmetric and anti-symmetric spatial impulse responses that allow the extraction of local properties of symmetry in particular directions. Control over angular selectivity is also very relevant, and we have sought prototype angular functions that allow bandpass channel orientation selectivity to be readily tuned.

The prototype general angular frequency characteristic

$$\Phi_0(\phi) = \cos^3(\phi)\ \mathrm{rect}(\phi/\pi) \tag{4}$$

has been used, where $\mathrm{rect}(\phi/\pi) = U(\phi + \tfrac{1}{2})U(\tfrac{1}{2} - \phi)$ and $U(\cdot)$ is the unit step function.

The prototype angular frequency response is rotated to generate the angular characteristics of oriented filters for a full filter set by the following:

$$\Phi_{0,k}(\phi) = \Phi_0(\phi - \phi_k) \tag{5}$$

The number of unique filter kernels necessary to implement this choice of a $K = 8$ filter set is only 4. Accordingly, the angular characteristics of the filter in the Fourier domain satisfy the following.

$$\sum_{k=0}^{k.2-1} \Phi_{0,k}(\phi)\,\Phi_{1,k}(\phi) + \Phi_{0,k}(\phi+\pi)\Phi_{1,k}(\phi+\pi) = C_\phi \tag{6}$$

To obtain near PR across the angular selective band pass filter channels, it is useful to have C_ϕ as close as possible to a constant value. This is similar to the frame reconstruction requirements of decompositions addressed in [9]. Correction can be made for non-uniform $C_\phi(\phi)$ in a post-filtering step.

2.4 Steering and Orientation Estimation

The steerable filtering framework allows both orientation adaptive filtering and orientation estimation to be performed in one framework. At the ℓth level of pyramidal decomposition, we wish to combine the outputs of K fixed bandpass filters at K orientations, in order to synthesize an output from a bandpass filter that is oriented at some angle ϕ_s. Let $f_k^{(\ell)}(m, n)$, $k = 0, 1, \ldots, K$, denote the output of the kth bandpass filter at level ℓ. First, note that, due to the nature of 2-D Fourier space, the outputs of the filters corresponding to $k = K/2, K/2+1, \ldots K-1$ are provided by the complex conjugates of the out puts of filters in the range $k = 0, 1, \ldots, K/2-1$. Specifically, we have

$$f_{k+K/2}^{(\ell)}(m,n) = \left(f_k^{(\ell)}(m,n)\right)^*, \quad k = 0, 1, \ldots, K/2-1 \tag{7}$$

If the angle that we wish to steer the filters to is denoted by ϕ_s, then we compute the steered output $f_s^{(\ell)}(m, n\ \phi_s)$ of the bandpass filters at levelof the decomposition by

$$f_s^{(\ell)}(m,n,\phi_s) = \sum_{k=0}^{K/2-1} s_p(\phi,k)\ f_k^{(\ell)}(m,n) + \sum_{k=0}^{K/2-1} s_q(\phi,k)\left(f_k^{(\ell)}(m,n)\right)^* \tag{8}$$

The functions $s_p(\phi, k)$ and $s_q(\phi, k)$ are the polynomial steering functions and they control the weights given to the K fixed filters by exploiting the relation of (7). The steering functions are compactly represented by using the coefficients p_k and q_k of the polynomial fits in steered angle ϕ_s, to the steering weights as determined by.

$$s_p(\phi,k) = \sum_{n=1}^{p} p_k(n)\phi^n \text{ and } s_q(\phi,k) = \sum_{n=1}^{q} q_k(n)\phi^n \tag{9}$$

3. GENERATING FEATURE MAPS

In this section we describe the orientation maps, Corner Likelihood Response and phase estimation in brief and are as follows.

3.1 Orientation Maps

One of the primary aims of the filter design is the construction of the bandpass filters in required orientation dominance for visual attention particularly for medical imaging. A measure of *orientation dominance* has been constructed using the idea of circular variance. This notion, employed, for example in [10] for characterizing the angular tuning of orientation-selective cells in the primary visual cortex of mammals, provides a measure quite similar to the principal eigenvector of the Hessian, used in scale-space techniques [11]. Based on this measure, we construct an orientation dominance complex field as follows:

$$O^{(\ell)}(m,n) = \frac{\sum_{k=0}^{K/2-1} |f_k^{(\ell)}(m,n)|\, e^{j2\phi_k}}{p + \left(\sum_{k=0}^{K/2-1} |f_k^{(\ell)}(m,n)|^2\right)^{\frac{1}{2}}} \tag{10}$$

where the conditioning constant p is set at 1.25% of the maximum value in the image being decomposed.

3.2 Corner Likelihood Response

The outputs of the filters may be used to generate a measure that may be associated with the likelihood of a particular location in an image being the corner of some structure. We construct the corner feature map

$$C^{(\ell)}(m,n) = \frac{\prod_{k=0}^{K/2-1} \left|f_k^{(\ell)}(m,n)\right|}{p + \left(\sum_{k=0}^{K/2-1} \left|f_k^{(\ell)}(m,n)\right|\right)^{K/2}} \tag{11}$$

The map produced by (11) uses the product of the magnitude of responses from individual filters sensitized to different directions, yielding a strong response only if all filters have a strong response. The design of the kernels is important here, though the energy is measured in a particular radial frequency band corresponding to the scale of the decomposition, to prevent arbitrary point-noise sources from yielding strong responses. Also, the denominator normalizes the response to local anisotropic energy.

To illustrate the principle, Fig. 2(a) shows a well-known scene containing toy blocks. The measure overlaid on Fig. 2(b), is given by

$$C^{(2)}_{\text{Likelihood}}(m,n) = C^{(2)}(m,n)\, I^{(1)}(m,n) \tag{12}$$

where $I(\ell)$ is an isotropic measure of local energy in the ℓth subband of radial frequency. It is generated from filter outputs by

$$I^{(\ell)}(m,n) = \left(\sum_{k=0}^{K/2-1} \left| f_k^{(\ell)}(m,n) \right|^2 \right)^{1/2} \tag{13}$$

Bilinear interpolation is used to align feature maps at different scales.

3.3. Phase Estimation

Phase estimates extracted from the steerable filters provide a means of feature extraction. Examples on the use of phase as an image feature can be found in [12], [1] and [13]. We apply the technique of steered phase estimation to construct a likelihood image for edges of particular structures. In the example of this section, we construct measures of edge structure likelihood and of interior structure likelihood, both extracted from different scales of decomposition of a simple image of rice grains. The phase estimate $\psi_s^{(\ell)}(m, n)$ is obtained from the argument of the complex filter outputs $f_s^{(\ell)}(m, n, \phi_s)$,

$$\psi_s^{(\ell)}(m, n) = \arg\left(f_s^{(\ell)}(m, n, \phi_s) \right) \tag{14}$$

Our proposed edge likelihood function at location (m, n), which is quite specific to this problem, is formulated as

$$\frac{\Gamma_e^{(1)}(m,n)\left(0.001 + C^{(1)}(m,n)C^{(2)}(m,n)\right)}{0.01 + \Gamma_b^{(2)}(m,n) + \Gamma_b^{(3)}(m,n)} \tag{15}$$

where

$$\Gamma_e^{(\ell)}(m,n) = O_d^{(\ell)}(m,n)\cos\left(\psi_s^{(\ell)}(m,n) + \pi\right) \quad , \quad U\left(\cos\left(\psi_s^{(\ell)}(m,n) + \pi\right)\right) \tag{16}$$

$$\Gamma_b^{(\ell)}(m,n) = O_d^{(\ell)}(m,n)\cos\left(\psi_s^{(\ell)}(m,n)\right) U\left(\cos\left(\psi_s^{(\ell)}(m,n)\right)\right)$$

and, $U(\cdot)$ is the unit step function.

3.4 Edge Structures Estimation

The measure of edge likelihood (15) is designed by noting that edge pixels are $\pm\pi$ likely to have a phase of radians at a fine scale of band pass filtering, coupled with a strong orientation dominance; this leads to Γ_e the term in the numerator of (15) defined as in (16). Because a pure phase response will tend to "ring" around an edge, the overall likelihood function is decreased by penalty terms that effectively suppress this ringing. The penalty terms in $\Gamma_b^{(\ell)}(m, n)$ utilize the observation that the interiors of objects will display a phase close to zero at the coarser scales (here, scales 2 and 3), together with strong orientation dominance at these scales. Because the strength of the orientation dominance decreases near to a corner, the corner similarity measures of (11) derived from scales 1 and 2, ($C^{(1)}(m, n)$ and $C^{(2)}(m, n)$), are used to boost the likelihood response as shown in the numerator of (16).

The corner response used is illustrated in Fig.3(a), and the final edge likelihood function is superimposed on the original image in Fig. 3(b). No edge-linking or post processing has been used to produce these images, apart from gating on the red color channel.

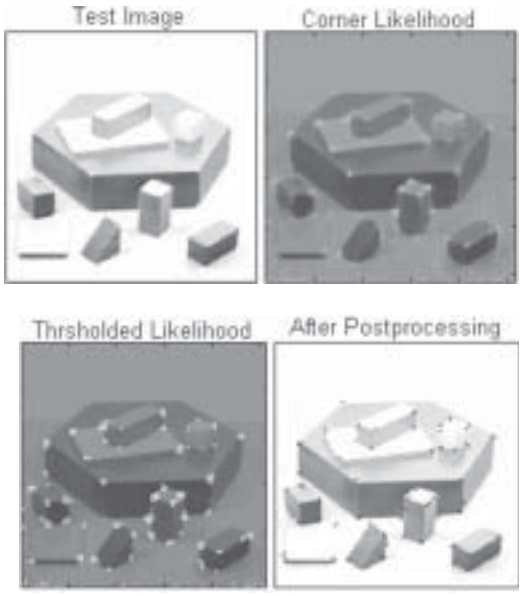

Figure 2: (a) Original image. (b) Measure $C^{(2)}_{\text{Likelihood}}$, superimposed on original image. (c) $C^{(2)}_{\text{Likelihood}}$ thresholded at 0.2, to yield a binary region mask. (d) After post-processing applied to (c) which consists of connected components labeling, finding the centroid by binary moments, and sketching a circle around the centroids.

4. IMAGE DENOISING ALGORITHM

For the past two decades image denoising has been demonstrated in the wavelet domain using techniques involving soft thresholding approaches, also known as wavelet coring and wavelet shrinkage in the literature [14-18]. In this paper we use *Steered Complex Shrinkage*

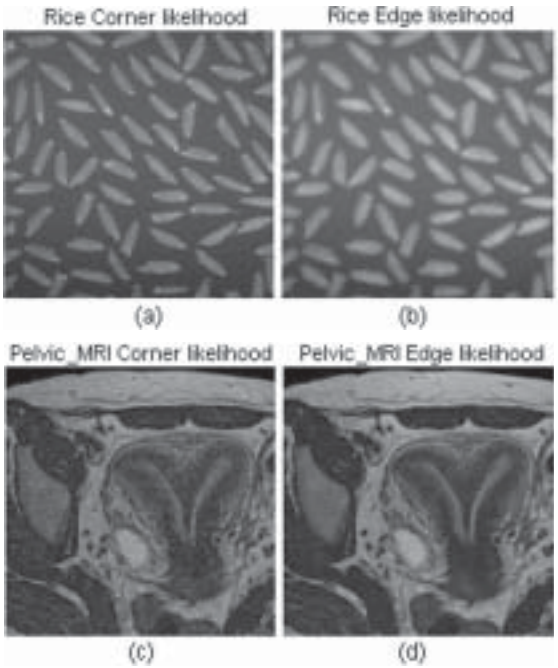

Figure 3: (a)&(c) Corner likelihood response (18) in red, (b)&(d) Edge likelihood function (15) in red superimposed on the rice grain and Pelvic_MR image.

technique that utilizes the feature maps suggested in previous sections. The denoising, thus, takes the form of a structure-driven technique, which smoothes along edges, and, at coarse scales, preserves corner structures. The approach is as follows and the various stages of the algorithm are illustrated in Fig. 4.

(1) Decompose the noisy image into subbands as follows.

(a) A down sampled low-pass channel at the coarsest scale $\mathcal{D}f^{(L)}(m, n)$, where $\mathcal{D}$ represents a down sampling operator.

(b) L-level Obtain the orientation dominance field $O^{(\ell)}(m, n)$ for $\ell = 0, 1, \ldots L$ using (10). From this equation compute the dominant orientation map $\phi_s^{(\ell)}(m, n)$.

for $\ell = L: -1:0$

(2) Filter the bandpass channels $f_k^{(\ell)}(m, n)$ with the synthesis filter bank to reconstruct the unsteered image channels $\hat{f}_k^{(\ell)}(m,n)$.

(3) Steer the reconstructed image channels $\hat{f}_k^{(\ell)}(m,n)$ to obtain $\hat{f}_s^{(\ell)}(m,n)$ using (8) with the dominant orientation map $\phi_s^{(\ell)}(m, n)$.

(4) Upsample $\mathcal{D}f^{(\ell)}(m, n)$ and filter with the synthesis lowpass filter to obtain $\hat{f}^{(\ell)}(m,n)$.

(5) Generate a reconstructed version of the image at level $\ell - 1$ by a weighted summation of the reconstructed image at level ℓ, $f^{(\ell)}(m, n)$ the unsteered reconstructed image channels $\hat{f}_k^{(\ell)}(m,n)$, and the steered reconstructed image channel $\hat{f}_s^{(\ell)}(m,n)$.

$$\left(\mathcal{D}f^{(\ell-1)}\right)(m,n) = \alpha_1^{(\ell)}\hat{f}^{(\ell)}(m,n) + \alpha_2^{(\ell)}(m,n) \sum_{k=0}^{K/2-1} \hat{f}_k^{(\ell)}(m,n) + \alpha_3^{(\ell)}(m,n)\hat{f}_s^{(\ell)}(m,n) \quad (17)$$

where $\alpha_2^{(\ell)}(m,n) = G_2^{(\ell)}\gamma^{(\ell)}(\sigma)\left(O_d^{(\ell)}(m,n) + C^{(\ell)}(m,n)\right)$

and $\alpha_3^{(\ell)}(m,n) = G_3^{(\ell)}\left(1 - \gamma^{(\ell)}(\sigma)\left(1 + 0.4C^{(\ell)}(m,n)\right)\right)$

6. Then obtain the denoised image $\tilde{x}(m, n) = f^{(0)}(m, n)$.

end

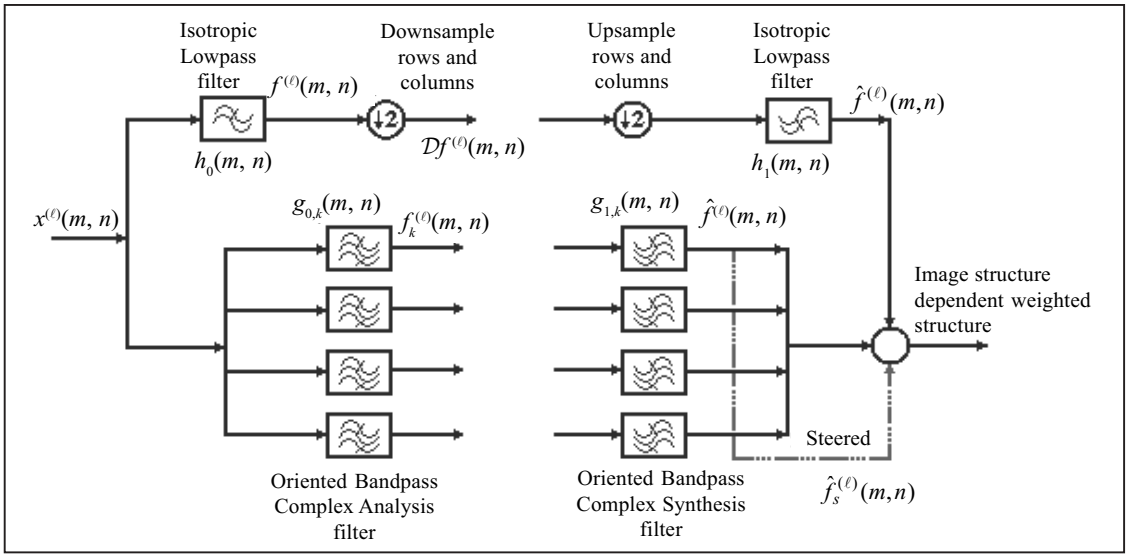

Figure 4: Illustration of the various stages of the denoising algorithm.

Some conditioning of the wavelet outputs is required prior to applying (10) in Step (2): A complex shrinkage is used across all scales, and the anisotropic measure (11) at the finest scale is weighted by the anisotropic measure at one scale above. More details of the complex shrinkage are to be found in, and, in particular (20). It should be stressed that these operations are *only* used to condition the anisotropy measure, and not for the noisy coefficients used in the steered reconstruction.

In (17) $\alpha_1^{(\ell)}$ is a gain function for the low-pass channel, which is usually very close to 1, $\alpha_2^{(\ell)}(m, n)$ is a field that adjusts the steered output to preserve edges at intermediate and coarse scales and $\alpha_3^{(\ell)}(m, n)$ is a field which preserves strong corner points at coarse scales in high noise, and at all scales in low-noise conditions. andare optimized once, and not altered with noise or images. The noise-dependent weights $\gamma^{(\ell)}(\sigma)$ alter the balance between steered and isotropic response depending on the estimated noise in the image. The effect of this sequence of operations is to smooth the image (by suppressing band pass output) in regions where there is little dominant orientation, and in cases of high noise. Where there is strong orientation dominance, however, the bandpass output is maintained as a steered response.

4.1 Steered Complex Shrinkage

For the shrinkage of coefficients in our complex wavelet decomposition, called *ComplexShrink*, we have applied the following mapping to the outputs of the analysis bandpass filter channels for all levels ℓ,

$$f_k^{(\ell)}(m,n) = \begin{cases} \left(\left|f_k^{(\ell)}(m,n)\right| - T^{(\ell)}\right) e^{\left(j\cdot\arg\left(f_k^{(\ell)}(m,n)\right)\right)}, & \left|f_k^{(\ell)}(m,n)\right| > T^{(\ell)} \\ 0, & \text{Otherwise} \end{cases} \tag{18}$$

The threshold $T^{(\ell)}$ was set to a value of 0.1 $0.1\left\|f_k^{(\ell)}(m,n)\right\|_\infty$, i.e., 10% of the maximum band pass output magnitude at each *scale*, and this was not changed during the experiments. Our suggested steered reconstruction called *Steered Complex Shrinkage* is based on the algorithm defined in (17).

5. COMPUTER SIMULATIONS AND RESULTS

A standard test pattern Shepp-Logan head phantom, a Thyroid CT Coronal image and a Pelvic MR images of sizes 512 × 512 each are used for the denoising purpose and elevating the important features such as edges, corners and orientations. An additive white Gaussian noise (AWGN) of variance, 30 is added to the original image to obtain noisy image. In the case of noisy image, noise variance is calculated using the median absolute variance (MAV) estimator σ_N = Median (|HH1|)/0.6745 of Donoho [15], where is the diagonal sub band of noisy image at scale 1. The *Steered Complex Shrinkage Algorithm* described in previous section with steerable filters is used for the denoising purpose. All the algorithms are implemented in Matlab. The results are compared with soft shrinkage technique in decimated discrete wavelet transform (Symmlet-8) called *Symmlet Shrinkage* in various forms are shown in Fig. 5 to Fig. 7. Fig. 8 shows the 256th horizontal line profile comparison for Shepp-Logan head phantom which clearly demonstrates the denoising performance using *Complex Shrinkage*. Table 1 shows the comparisons of widely used metrics such as Signal to Noise Ratio (SNR), Peak Signal to Noise Ratio (PSNR), and Improved Signal to Noise Ratio (ISNR). The results show that the proposed algorithm improves in SNR

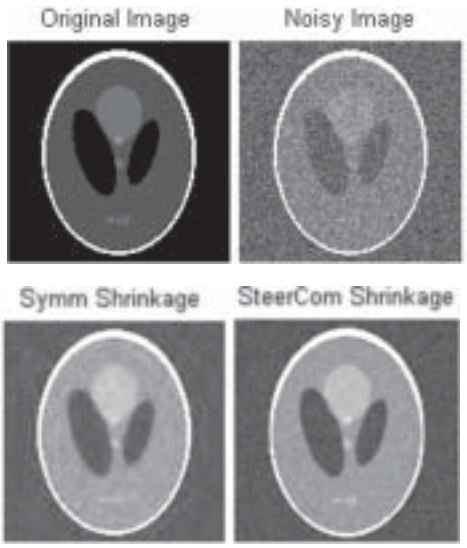

Figure 5: (a) Original Shepp-Logan Head Phantom (b) Noisy Image Corrupted with AWGN of Variance 30. (c) Denoising using *Symmlet Shrinkage* (d) Denoising using Proposed *Steerable Complex Shrinkage* Algorithm

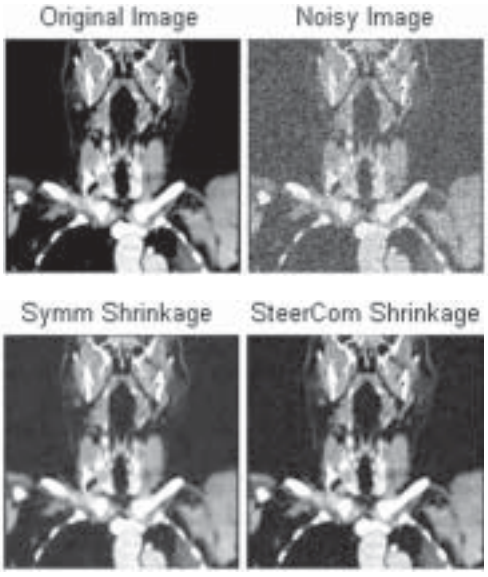

Figure 6: (a) Original Thyroid CT Coronal Image (b) Noisy Image Corrupted with AWGN of variance 30. (c) Denoising using *Symmlet Shrinkage* (d) Denoising using Proposed *Steerable Complex Shrinkage* Algorithm

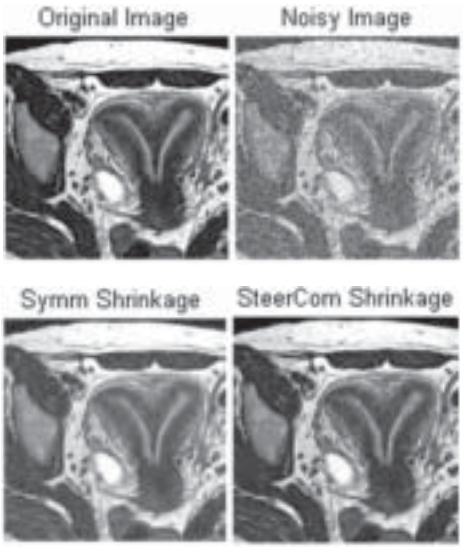

Figure 7: (a) Original Pelvic MR Image (b) Noisy Image Corrupted with AWGN of Variance 30. (c) Denoising using *Symmlet Shrinkage* (d) Denoising using Proposed *Steerable Complex Shrinkage* Algorithm

of 2.49dB over *Symmlet Shrinkage* for Pelvic MR Image. More over the visual appearance of edges, corners and orientations are improved in the proposed algorithm. The computation time for *Symmlet Shrinkage* is 0.4 seconds and additional 18.16 seconds for optimal shrinkage factor calculation, where as 9 seconds for the steered complex shrinkage in Intel Pentium 2.8 GHz with 512 MB RAM. The corner and edge orientation maps are also shown in Fig. 2. and Fig. 3.

6. CONCLUSIONS AND FURTHER RESEARCH

We proposed a new transform (wavelet) domain structure driven denoising technique called *Steerable Complex Shrinkage* which preserves the edges, corners and orientation features and application to medical images. For this purpose we used an efficient steerable complex pyramidal wavelet transform that uses pairs of complex steerable orientation bandpass filters. These complex filters have been engineered into a multirate system, providing a synthesis and analysis sub band filtering system with good reconstruction properties. The corner and edge orientation maps are shown in Fig. 2 and Fig. 3. The results for medical image denoising using the *Steerable Complex Shrinkage* algorithm is shown in Fig. 5 to Fig. 8 and Table.1. Our proposed algorithm improves not only in terms of signal to noise ratios and also enhances the edge and corner orientation features.

Our current denoising approach makes use of orientation and steered phase features from the bandpass channels only, and we have performed denoising and reconstruction *only* with these and the lowpass channel. While we can both increase the angular selectivity of our system and introduce highpass residual channels, we have chosen to keep the complexity of the filter bank system low in order to explore parallel hardware implementation. To obtain further improvements, it is also necessary to develop principled statistical models for the behavior of features under addition of noise, and their relationship to the uncorrupted wavelet coefficients. And also the proposed algorithm considered additive white Gaussian noise only. It is required to develop the algorithm for other noisy sources such as Poisson, Rician and Speckle are corrupted specifically in medical imaging.

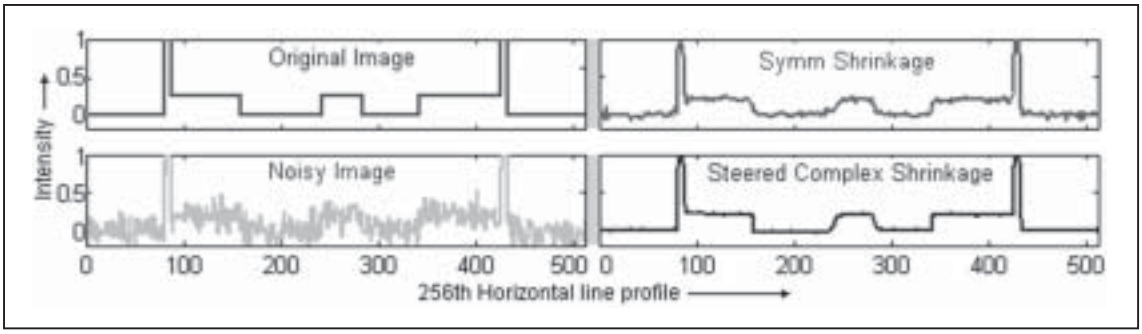

Figure 8: 256th Horizontal Line Profile Comparison for Shepp-Logan Head Phantom

Table 1
Signal to Noise Ratio Comparisons for Three Images

Reconstruction Technique	*Shepp-Logan Head Phanton*				*Pelvic MR image*				*Thyroid CT Coronal image*			
	MSE (dB)	*SNR (dB)*	*PSNR (dB)*	*ISNR (dB)*	*MSE (dB)*	*SNR (dB)*	*PSNR (dB)*	*ISNR (dB)*	*MSE (dB)*	*SNR (dB)*	*PSNR (dB)*	*ISNR (dB)*
Discrete Wavelet Transform	118.52	15.24	27.39	8.82	160.79	19.07	26.07	7.43	97.32	19.56	29.23	9.67
Steered Complex Shrinkage	91.77	16.39	28.53	9.96	90.74	21.55	28.56	9.98	58.86	21.74	31.42	11.86

REFERENCES

[1] W. T. Freeman and E. H. Adelson, "The Design and use of Steerable Filters," *IEEE Trans. Pattern Anal. Mach. Intell.*, **13**, (9), (Sep. 1991), 891–906.

[2] E. P. Simoncelli, W. T. Freeman, E. H. Adelson, and D. J. Heeger, "Shiftable Multi Scale Transforms," *IEEE Trans. Inf. Theory*, **38**, (2), (Mar. 1992), 587–607.

[3] N. Kingsbury, "Image Processing with Complex Wavelets," *Phil. Trans. Roy. Soc. London-Ser. A*, **357**, (1760), (Sep. 1999), 2543–2560.

[4] M. Venu Goapal Rao and S. Vathsal, ComForWaRD: Complex Fourier Wavelet Regularized Deconvolution in CT, International Conference on Computational Intelligence and Multimedia Applications, *IEEE Computer Society*, **3**, (2007), 240–44.

[5] T. C. Folsom and R. B. Pinter, "Primitive Features by Steering, Quadrature, and Scale," *IEEE Trans. Pattern Anal. Mach. Intell.*, **20**, (11), (Nov. 1998), 1161–1173.

[6] L. Sendur and I. W. Selesnick, "Bivariate Shrinkage Functions for Wavelet-based Denoising Exploiting Interscale Dependency," *IEEE Trans. Signal Process.*, **50**, (11), (Nov. 2002), 2744–2756.

[7] A. A. Bharath and Jeffry. Ng, "A Steerable Complex Wavelet Construction and Its Application to Image Denoising", *IEEE Trans. On. Image Processing*, **14**, (7), (July 2005).

[8] A. A. Bharath, "Steerable Filters from Erlang Functions," in *Proc. 9th Brit. Machine Vision Conf.*, (1998), 144–153.

[9] I. Daubechies, "The Wavelet Transform, Time-frequency Localization, and Signal Analysis," *IEEE Trans. Inf. Theory*, **36**, (5), (Sep.1990), 961–1005.

[10] D. L. Ringach, R. M. Shapley, and M. J. Hawken, "Orientation Selectivity in Macaque V1: Diversity and Laminar Dependence," *J. Neurosci.*, **22**, (3), (Jul. 2002), 5639–5651.

[11] M. E. Martínez-Perez, A. D. Hughes, A. V. Stanton, S. A. Thom, A. A. Bharath, and K. H. Parker, "Segmentation of Retinal Blood Vessels based on the Second Directional Derivative and Region Growing," in *Proc. Int. Conf. Image Processing*, **2**, (1999), 173–176.

[12] P. Kovesi, "Image Features from Phase Congruency," *Videre: J. Comput. Vis. Res.*, **1**, (3), (1999), 1–26.

[13] M. C. Morrone and D. C. Burr, "Feature Detection in Human Vision: A Phase Dependent Energy Model," in *Proc. Roy. Soc. London, B*, **235**, (1988), 221–245.

[14] S. G. Chang, Y. Bin, and M. Vetterli, "Adaptive Wavelet Thresholding for Image Denoising and Compression," *IEEE Trans. Image Process.*, **9**, (9), (Sep. 2000), 1532–1546.

[15] D. L. Donoho, "Denoising by Soft Thresholding," *IEEE Trans. Inf. Theory*, **41**, (3), (May 1995), 613–627.

[16] J. Scharcanski, C. R. Jung, and R. T. Clarke, "Adaptive Image Denoising using Scale and Space Consistency," *IEEE Trans. Im. Process.*, **11** (9), (Sep. 2002), 1092–1101.

[17] I. W. Selesnick, "A New Complex-directional Wavelet Transform and its Application to Image Denoising," in *Proc. Int. Conf. Image Processing*, **3**, (2002), 573–576.

[18] E. P. Simoncelli and E. H. Adelson, "Noise Removal via Bayesian Wavelet Coring," in *Proc. Int. Conf. Image Processing*, **1**, (Sep. 1996), 379–382.

[19] J. Canny, "A Computational Approach to Edge Detection," *IEEE Transactions on Pattern Analysis and Machine Intelligence*, **8**, (6), 1986.

[20] P. Perona, "Orientation Diffusions," *IEEE Transactions on Image Processing*, **7**, (3), (1998), 457–467.

[21] X.G. Feng and P. Milanfar, "Multiscale Principal Components Analysis for Image Local Estimation," in *The 36th Conference on Signals, Systems and Computers*, Pacific Grove, USA, (November 2002), **1**, 478–482.